J Neurophysiol 114: 2404–2417, 2015.
First published July 22, 2015; doi:10.1152/jn.00577.2015.

Syntaxin 1B is important for mouse postnatal survival and proper synaptic function at the mouse neuromuscular junctions

Yuan-Ju Wu,[1] Rocio Tejero,[2] Marife Arancillo,[1] Gülcin Vardar,[1] Tatiana Korotkova,[1,3] Michael Kintscher,[1] Dietmar Schmitz,[1] Alexey Ponomarenko,[1,3] Lucia Tabares,[2] and Christian Rosenmund[1]

[1]*NeuroCure Cluster of Excellence, Charité-Universitätsmedizin Berlin, Berlin, Germany;* [2]*Department of Medical Physiology and Biophysics, School of Medicine, University of Seville, Seville, Spain; and* [3]*Leibniz Institute for Molecular Pharmacology, Berlin, Germany*

Submitted 10 June 2015; accepted in final form 21 July 2015

Wu YJ, Tejero R, Arancillo M, Vardar G, Korotkova T, Kintscher M, Schmitz D, Ponomarenko A, Tabares L, Rosenmund C. Syntaxin 1B is important for mouse postnatal survival and proper synaptic function at the mouse neuromuscular junctions. *J Neurophysiol* 114: 2404–2417, 2015. First published July 22, 2015; doi:10.1152/jn.00577.2015.—STX1 is a major neuronal syntaxin protein located at the plasma membrane of the neuronal tissues. Rodent STX1 has two highly similar paralogs, STX1A and STX1B, that are thought to be functionally redundant. Interestingly, some studies have shown that the distribution patterns of STX1A and STX1B at the central and peripheral nervous systems only partially overlapped, implying that there might be differential functions between these paralogs. In the current study, we generated an STX1B knockout (KO) mouse line and studied the impact of STX1B removal in neurons of several brain regions and the neuromuscular junction (NMJ). We found that either complete removal of STX1B or selective removal of it from forebrain excitatory neurons in mice caused premature death. Autaptic hippocampal and striatal cultures derived from STX1B KO mice still maintained efficient neurotransmission compared with neurons from STX1B wild-type and heterozygous mice. Interestingly, examining high-density cerebellar cultures revealed a decrease in the spontaneous GABAergic transmission frequency, which was most likely due to a lower number of neurons in the STX1B KO cultures, suggesting that STX1B is essential for neuronal survival in vitro. Moreover, our study also demonstrated that although STX1B is dispensable for the formation of the mouse NMJ, it is required to maintain the efficiency of neurotransmission at the nerve-muscle synapse.

SNARE; NMJ; neurotransmitter release; spontaneous release; evoked release

IN NEURONS, SYNAPTIC TRANSMISSION is initiated by action potential-mediated exocytosis at the active zone (Rizo and Rosenmund 2008). Like the fusion processes of other vesicular transport in cells, synaptic transmission is tightly regulated by the soluble *N*-ethylmaleimide-sensitive factor attachment protein receptor (SNARE) complex and Sec/Munc18-like (SM) proteins (Hong and Lev 2014). The neuronal SNARE complex consists of synaptobrevin-2 [SYB2; as a vesicle (v-) SNARE located on the synaptic vesicle membrane] and syntaxin 1 (STX1) and synaptosomal-associated protein 25 [SNAP-25; both proteins are the target (t-) SNAREs located on the plasma membrane; Rizo and Rosenmund 2008; Rizo and Südhof 2012].

The importance of the neuronal SNARE complex for neurotransmitter release has been demonstrated in both in vitro and in vivo systems. Cleavage of SNAP-25 by botulinum toxin A in rat primary neuronal cultures (Peng et al. 2013) and cleavage of SNAP-25 and STX1 by botulinum toxins A and C, respectively, and SYB2 by tetanus toxin in rat calyx of Held all showed severe reduction of neurotransmitter release (Sakaba et al. 2005). Loss of either SYB2 or SNAP-25 by genetic modification in organisms, such as *Drosophila*, *Caenorhabditis elegans*, and *Mus musculus*, resulted in early lethality. Neuromuscular junctions (NMJs) from mutant *Drosophila* and *C. elegans* organisms or neurons derived from knockout (KO) mice all displayed severe impairments of synaptic transmission (Deitcher et al. 1998; Nonet et al. 1998; Schoch et al. 2001; Vilinsky et al. 2002; Washbourne et al. 2002). Depletion of STX1 in *Drosophila* and *C. elegans* also caused embryonic lethality as well as an entire abolishment in neurotransmitter release (Saifee et al. 1998; Schulze et al. 1995).

In the mammalian systems, two paralogs of STX1 exist, 1A and 1B. Since STX1A and STX1B share an 84% amino acid homology (Bennett et al. 1992) and common functional domains, such as a large NH_2-terminal Habc domain, a SNARE domain, a linker region, and a COOH-terminal transmembrane domain (Rizo and Rosenmund 2008), it has been suggested that STX1A and STX1B are functionally redundant. Indeed, two independently generated STX1A KO mice showed a normal life span, and hippocampal neurons isolated from those mice exhibited similar neurotransmission compared with the control, indicating that STX1B functionally compensates the role of STX1A (Fujiwara et al. 2006; Gerber et al. 2008). However, complete loss or partial loss of STX1B in mice caused a preweaning death, suggesting that STX1A and STX1B have differential functions (Arancillo et al. 2013; Kofuji et al. 2014; Mishima et al. 2014). Mishima et al. (2014) have recently suggested that STX1B but not STX1A is necessary for the regulation of spontaneous and evoked synaptic transmission in hippocampal neurons. In contrast, Arancillo et al. (2013) have demonstrated that STX1A and STX1B rescued the neurotransmission to a similar degree in autaptic hippocampal neurons with a low copy number of STX1, arguing against a differential role between these two paralogs in the neurotransmission in hippocampal neurons.

Address for reprint requests and other correspondence: C. Rosenmund, Charité-Universitätsmedizin Berlin, Charitéplatz 1, 10117 Berlin, Germany (e-mail: christian.rosenmund@charite.de).

Moreover, Ruiz-Montasell et al. (1996) and Aguado et al. (1999) have shown that the expression patterns of STX1A and STX1B examined in the central nervous system (CNS) and peripheral nervous system (PNS) in adult rodents do not completely overlap. This could imply that STX1B may be important in synapses other than hippocampal neurons. However, almost all cellular and biochemical studies of STX1 have focused on hippocampal neurons. Therefore, in this current study, we addressed the question of whether STX1B has a distinct function from STX1A by generating an STX1B KO mouse line and by investigating several regions in both CNS and PNS in the STX1B KO mice. We confirmed that, unlike STX1A, removal of STX1B in mice is lethal. We further demonstrated that STX1B is an important paralog in the mouse NMJs and loss of STX1B in mice resulted in an impaired neurotransmission at the NMJs.

MATERIALS AND METHODS

Generation of STX1B KO mouse line and STX1B floxed mouse line. A BAC clone containing the genomic region spanning STX1B was obtained from the bMQ Mouse BAC library (Adams et al. 2005). LoxP sites were introduced between the exon 1 and exon 5, and a neomycin cassette with FRT sites was introduced between the exon 4 and the 3′ loxP site. The fragment containing loxP sites and the neomycin cassette was subcloned into a modified P[acman] vector (Venken et al. 2006). The linearized targeting vector (Fig. 1) was electroporated into AB2.2 embryonic stem cells. Positive clones were screened by Southern blotting and injected into C57BL/6 blastocytes. Chimeric offspring were backcrossed to C57BL/6 mice. Progeny were crossed to HPRT-Cre deleter mice to obtain mice with an STX1B KO allele (Nichol et al. 2011). First-generation STX1B knockouts were backcrossed again to C57BL/6, and STX1B heterozygous (Het) offspring were intercrossed to generate the STX1B KO colony.

To remove the FRT-flanked neomycin cassette for generating the STX1B floxed (FL) mouse line, mice from the backcrossed progeny were crossed to ROSA-FLP deleter mice (Farley et al. 2000) in a C57BL/6 background (The Jackson Laboratories).

Animal maintenance. All protocols for animal maintenance and experiments were approved by and followed the regulations of Berlin authorities and the animal welfare of Charité-Universitätsmedizin Berlin and the European Council Directive for the Care of Laboratory Animals.

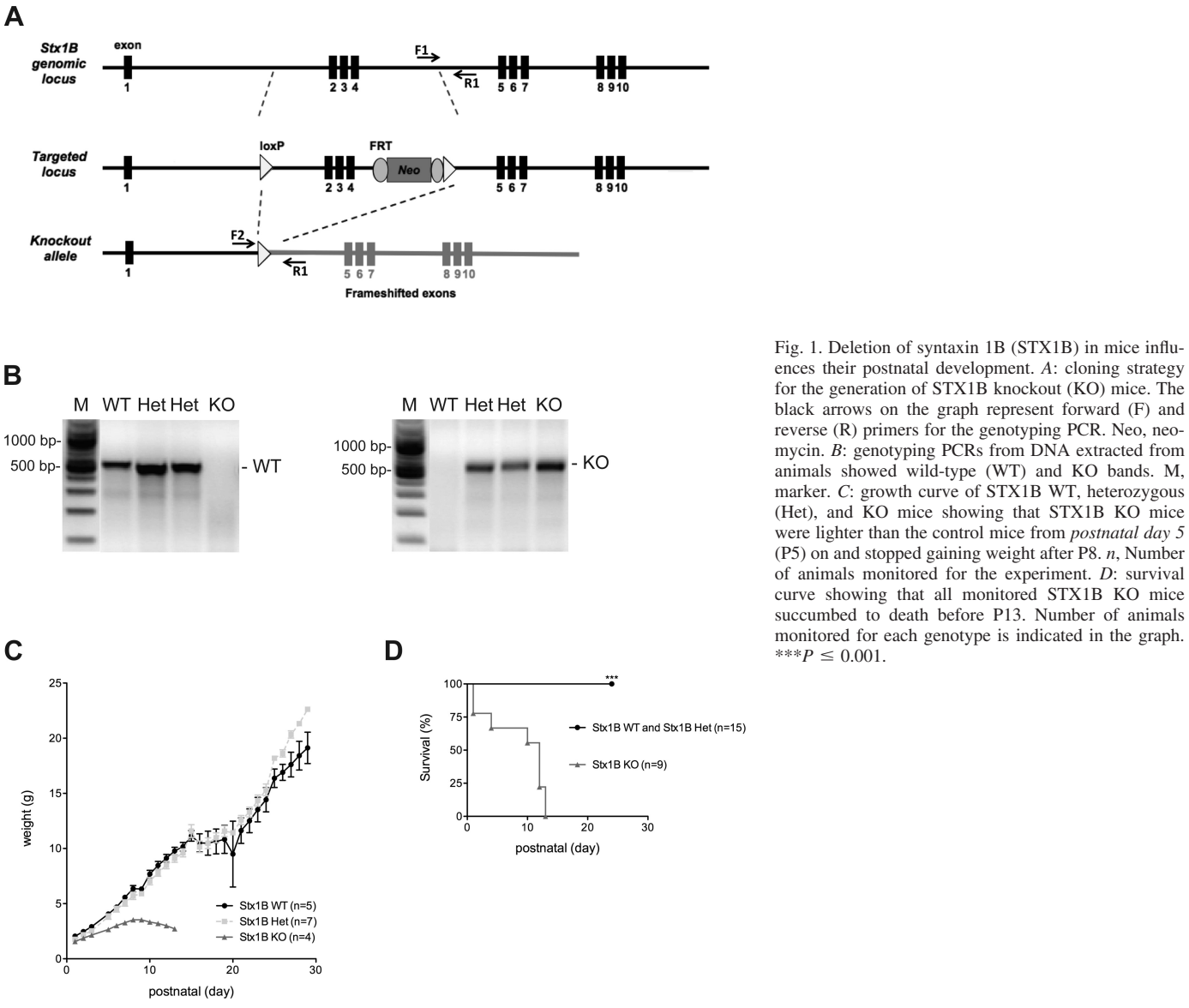

Fig. 1. Deletion of syntaxin 1B (STX1B) in mice influences their postnatal development. *A*: cloning strategy for the generation of STX1B knockout (KO) mice. The black arrows on the graph represent forward (F) and reverse (R) primers for the genotyping PCR. Neo, neomycin. *B*: genotyping PCRs from DNA extracted from animals showed wild-type (WT) and KO bands. M, marker. *C*: growth curve of STX1B WT, heterozygous (Het), and KO mice showing that STX1B KO mice were lighter than the control mice from *postnatal day 5* (P5) on and stopped gaining weight after P8. *n*, Number of animals monitored for the experiment. *D*: survival curve showing that all monitored STX1B KO mice succumbed to death before P13. Number of animals monitored for each genotype is indicated in the graph. $***P \leq 0.001$.

DNA analysis. Genomic DNA was extracted from the brains or from the ear biopsies of the mice using SNET lysis buffer containing proteinase K. PCR with forward (F1) and reverse (R1) primers containing a STX1B-specific sequence (F1: 5′-GTT TCC GCC TGA ATT GCA CCT G-3′; R1: 5′-CTG GCA CCA GCA GAC AAG GAG-3′) could amplify the STX1B wild-type (WT) allele with a ~500-bp band. A band with ~550 bp from the STX1B KO allele could be amplified with another forward (F2) primer and the R1 reverse primers (F2: 5′-CAT AGC CTG TCT GAC TTC CAG-3′).

Dissociated cell culture. Autaptic primary neuronal cultures from the hippocampus or striatum were prepared from newborn [*postnatal day* (P) *0-2*] mice, and the neurons were plated on astrocyte feeder layer microislands as previously described (Arancillo et al. 2013). Cultures with different genotype are generated from siblings that are treated identically during culturing. In addition, hippocampal and striatal cultures were incubated at 37°C for 12–16 days before performing further experiments. High-density dissociated cerebellar cultures containing both excitatory and inhibitory neurons were prepared from P5 to P7 mice using the method adapted from previous studies (Bilimoria and Bonni 2008; Facci and Skaper 2012). Briefly, cerebella from mice were removed and enzymatically and mechanically dissociated. Neurons were cultured on previously prepared astrocyte feeder cultures in Neurobasal-A media containing B-27 Supplement, 10 IU/ml penicillin, 1 μg/ml streptomycin, 2 mM L-alanyl-L-glutamine, and 20 mM KCl. The seeding density was 5.4×10^4 cells/cm^2. Dissociated cerebellar cultures were incubated at 37°C for 9–11 days before conducting further experiments.

Electrophysiology on dissociated cell cultures. Whole cell voltage-clamp recordings from autaptic hippocampal excitatory and striatal inhibitory neurons or high-density cerebellar cultures were obtained between *days in vitro* (DIV) *12-16* or *9-11*, respectively, at room temperature. The recordings and the analysis of the data were done as previously described (Arancillo et al. 2013). Extracellular solution contained in mM: 140 NaCl, 2.4 KCl, 10 HEPES, 10 glucose, 2 $CaCl_2$, and 4 $MgCl_2$. The patch pipette internal solution contained in mM: 136 KCl, 17.8 HEPES, 1 EGTA, 4.6 $MgCl_2$, 4 ATP-Na_2, 0.3 GTP-Na_2, 12 creatine phosphate, and 50 U/ml phosphocreatine kinase. Both extracellular and internal solutions were adjusted to pH 7.4 and the osmolarity ~300 mosM.

To block glutamatergic or GABAergic responses in autaptic cultures, 3 mM kynurenic acid and 30 μM bicuculline, respectively, were added to the extracellular solution. Sucrose solution (500 mM) was applied for 5 s to assess the size of the readily releasable pool (RRP; Rosenmund and Stevens 1996).

During the recording of the high-density cerebellar cultures, voltage-gated sodium channel blocker TTX (0.5 μM) was added in all of the extracellular solution. To block glutamatergic or GABAergic responses in these experiments, 5 μM 2,3-dioxo-6-nitro-1,2,3,4-tetrahydrobenzo[*f*]quinoxaline-7-sulfonamide (NBQX) and 30 μM bicuculline, respectively, were additionally added to the extracellular solution. To address the vesicle fusogenicity, hypertonic solutions were prepared as 150, 250, and 500 mM sucrose, and the application duration of each sucrose solution was 10, 8, and 5 s, respectively.

Borosilicate glass pipettes had a resistance of 2.5–4 MΩ. All recordings were performed with a MultiClamp 700B amplifier, and the data were acquired with Clampex 10.0 (Molecular Devices).

Evoked excitatory (EPSC) and inhibitory (IPSC) postsynaptic currents were recorded after depolarization from −70 to 0 mV for 2 ms. Vesicular release probability (P_{vr}) was determined by calculating the EPSC charge over the RRP charge of individual neurons. Spontaneous release was determined as miniature postsynaptic currents and was recorded for 60 s at −70 mV. To subtract background noise, recording was performed with the application of either kynurenic acid or bicuculline for the same time duration. Traces were filtered at 1 kHz, and events were detected by using a template-based algorithm in AxoGraph X. During each experiment, we acquired all genotype data on the same day. Moreover, we combined for each experiment from at least three independent cultures.

Transversus abdominis neuromuscular preparation. Mice were euthanized by exsanguinations according to the guidelines of the European Council Directive for the Care of Laboratory Animals. The mouse was positioned in dorsal decubitus, and the abdominal skin was opened through a midline incision and pulled to the sides. The whole left hemi-abdominal muscle wall, up to the sternum, was cut out and pinned to the bottom of a 2-ml chamber over a bed of cured silicone rubber (Sylgard; Dow Corning). As the transversus abdominis (TVA) is the inner muscle of the abdominal wall, the obliquus externus muscle and the fat tissue were removed carefully to obtain a free area of intact TVA muscle fibers. Care was taken to dissect the TVA corresponding nerve branch intact. The dissection was performed in a physiological solution containing, in mM, 135 NaCl, 12 $NaHCO_3$, 5 KCl, 1 $MgCl_2$, 2 $CaCl_2$, and 30 glucose, continuously gassed with 95% O_2-5% CO_2 (pH 7.35). After the dissection, the TVA muscle was incubated in clean-gassed solution for 30 min before performing the electrophysiological recordings.

Electrophysiology on NMJs. Intracellular recording from the TVA muscle was performed as previously described (Ruiz et al. 2010). Briefly, miniature (mEPP) and evoked end-plate potentials (EPPs) were recorded from STX1B WT, Het, and KO mice at P8. The nerve was electrically stimulated by a suction electrode. The stimulation consisted of square-wave pulses of 0.2 ms and 2–40 V, at 0.5 and 20 Hz of frequency. A glass microelectrode (10–30 MΩ) filled with 3 M KCl solution was connected to an intracellular recording amplifier (TEC-05X; NPI). Muscle contraction was blocked with μ-conotoxin GIIIB (2–4 μM; Alomone), a specific blocker of skeletal muscle voltage-gated sodium channels.

The mean amplitudes of the EPPs and mEPPs recorded at each fiber were linearly normalized to −70 mV. EPP amplitudes were corrected for nonlinear summation (Martin 1955). Quantal content was estimated by the direct method, obtained by the ratio between mean EPP and mean mEPP amplitudes. The kinetics of EPP and mEPP were measured by their decay time constant (exponential fit of the decay phase).

All NMJ electrophysiological data are given as mean values ± SE with *n* being the number of muscle fibers per group and *N* being the number of mice per group.

Electroencephalography recordings in freely moving mice using implanted intracranial epidural electrodes. Single tungsten wires (40 μm; California Fine Wire) were implanted on P15–P16 under isoflurane anesthesia. Craniotomies were performed without damaging the underlying dura. Electrodes were placed bilaterally at 2.0 mm posterior from bregma and 3.0 mm lateral from midline with a reference electrode above the cerebellum. Implanted electrodes were secured on the skull with dental acrylic. During recordings, electrodes were connected to operational preamplifiers; electrophysiological signals were differentially amplified, band-pass filtered (1 Hz to 10 kHz), and acquired continuously at 32 kHz (Neuralynx). Recordings were performed on freely moving animals at P15–P16 in Plexiglas cages 19 × 29 cm. EEG was obtained by low-pass filtering and downsampling of the wide-band signal to 1,250 Hz.

Brain slice preparation and Nissl staining. Animals used for Nissl staining or immunocytochemical analysis were deeply anesthetized and intracardially perfused with 0.9% NaCl followed by 4% paraformaldehyde (PFA) in 0.1 M sodium phosphate buffer (PB). Brains were removed and immersed in 4% PFA at 4°C overnight. To impede the formation of ice crystals during cryopreservation, fixed brains were immersed subsequently in 0.4 and 0.8 M sucrose in 0.1 M PB at 4°C overnight. Brains were preserved in Tissue-Tak, snap-frozen in *n*-hexane at −70°C, and cryosectioned with Leica cryostat to 25 μm/slice. Every sixth slice was selected for Nissl staining to determine the gross brain structure. Nissl-stained images were obtained with an Olympus (Tokyo, Japan) SZX16 research stereo

microscope with an Olympus DP70 digital camera. Remaining slices were preserved in antifreeze solution at −20°C and used later for immunocytochemistry.

Immunocytochemistry. To examine the staining pattern of the brain, PFA-perfused brain slices were removed from the antifreeze solution and washed 2 times with 1× PBS. Slices were permeabilized and blocked with 1× PBS containing 10% normal donkey serum (NDS) and 0.3% Triton X-100 for 30 min at room temperature. Slices were then incubated with primary antibodies at 4°C overnight [anti-STX1B and anti-Tau (both from Synaptic Systems)]. Next day, slices were incubated with fluorophore-conjugated secondary antibodies (Jackson ImmunoResearch) at dark for 1 h at room temperature. Finally, slices were embedded with mounting buffer and coverslipped.

To determine the neuronal number and vesicular glutamate transporter 1 (VGlut1) and vesicular GABA transporter (VGAT) puncta in high-density dissociated cerebellar cultures, cells on coverslips were fixed with 4% PFA for 10 min at room temperature at DIV 11. Cells were permeabilized with 1× PBS containing 0.1% Tween 20 (PBS-T) for 3 times, 15 min each, and then blocked in 1× PBS-T containing 5% NDS for 1 h. Cells were incubated with primary antibodies at 4°C overnight [anti-NeuN (Millipore), anti-VGlut1 (Synaptic Systems), and anti-VGAT (Synaptic Systems)]. Next day, cells were incubated with fluorophore-conjugated secondary antibodies at dark for 1 h. Finally, coverslips were mounted onto glass slides. Images were taken with an Olympus IX81 epifluorescent microscope.

To examine the staining pattern of the NMJs, TVA muscles from STX1B WT and KO mice were dissected in physiological Ringer solution. Muscles were incubated for 30 min in Ringer solution bubbled with carbogen before fixing in 4% PFA for 90 min. The fixed tissues were then incubated with 0.1 M glycine in PBS for 30 min, permeabilized with 1% Triton X-100 in PBS for 90 min, and blocked with 5% bovine serum albumin for 3 h. Afterward, tissues were incubated with primary antibodies [anti-STX1A (Aviva) and/or anti-STX1B (Synaptic Systems)] at 4°C overnight. Next day, tissues were incubated in 0.05% Triton X-100 in PBS for 1 h followed by an incubation with fluorophore-conjugated secondary antibodies (Invitrogen) and 2.5 μg/ml rhodamine-α-bungarotoxin (BTX-Rho; Sigma) for 1 h. The stained tissues were then rinsed with 0.05% Triton X-100 in PBS for 90 min. Finally, muscles were mounted with SlowFade medium (Invitrogen).

NMJs were imaged with an upright Olympus FV1000 confocal laser scanning microscope.

Western blot. Brain lysates were collected from deeply anesthetized animals and were prepared in lysis buffer containing a cocktail of proteinase inhibitors. Equal amounts of the proteins from each sample were loaded on SDS-PAGE gels and subsequently were transferred to nitrocellulose membranes. Membranes were blocked in 5% milk and incubated with primary antibodies recognizing STX1A, STX1B, SNAP-25, SYB2, Munc18-1, Rab5, synaptotagmin-1 (SYT1), synaptophysin-1 (SYN1), Munc13-1, or β-tubulin III at 4°C overnight. Munc18-1 and β-tubulin III antibodies were both purchased from Sigma, and the other antibodies were from Synaptic Systems. Then, the membranes were incubated with horseradish peroxidase-conjugated secondary antibodies (Jackson ImmunoResearch). To detect the protein levels, ECL Plus Western Blotting Detection Reagents were used. The protein expression levels were then quantified with ImageJ software.

Statistical analysis. Bar graphs showing mean and standard error of mean were presented in this study. Data were first tested for a Gaussian distribution with D'Agostino and Pearson omnibus normality test. If the data passed the normality test, one-way ANOVA followed by Bonferroni multiple-comparison tests were performed. Otherwise, nonparametric Kruskal-Wallis test followed by Dunn multiple-comparison tests were used.

RESULTS

STX1B homozygous deletion in mice causes impaired postnatal survival. STX1B KO mouse line was generated by targeting a replacement vector containing loxP sites and an FRT-flanked neomycin resistance cassette into the STX1B endogenous locus via homologous recombination in the embryonic stem cells. Mice harboring this targeted locus were crossed to HPRT-Cre deleter mice to obtain a STX1B KO allele (Nichol et al. 2011; Fig. 1*A* and MATERIALS AND METHODS). Mice Het for STX1B were physically indistinguishable from WT littermates and were intercrossed to obtain STX1B homozygous deletion mice. DNA was extracted from the pups, and the genotyping PCR confirmed the presence of STX1B KO mice among the newborns (Fig. 1*B*). STX1B KO mice were viable and were indistinguishable from the control littermates at birth. However, in contrast to STX1A KO mice, which have shown to be healthy and to have normal life spans (Fujiwara et al. 2006; Gerber et al. 2008), STX1B KO mice grew more slowly than the control littermates, and they stopped gaining weight at around P8 (Fig. 1*C*). Moreover, similar to another independent STX1B KO mouse line reported recently (Kofuji et al. 2014), STX1B KO mice generated in our study also showed motor abnormalities after P8 as their limbs gradually became rigid. Eventually, these mice succumbed to death before the age of 2 wk (Fig. 1*D*).

Removal of STX1B in mice does not affect the gross brain morphology or the morphological organization of the NMJ. In the next step, we compared the gross brain morphology between STX1B WT and STX1B KO mice at P10. Nissl-stained brain slices revealed that the gross brain morphology of STX1B KO mice could form similarly to that of STX1B WT mice (Fig. 2*A*). Immunohistochemical analysis with an antibody recognizing the axonal marker, Tau, showed that the hippocampal and cerebellar axonal signal was comparable between the control and KO mice (Fig. 2*B*). In addition, the mossy fibers in the hippocampus and the molecular layer in the cerebellum in WT brain slices showed an enrichment of signal for STX1B (Fig. 2*B*). Furthermore, because of the motor abnormalities noticed in STX1B KO mice, we also analyzed the structure of the NMJs. NMJs from the TVA muscles were prepared from KO and control mice at P8 and labeled with BTX-Rho, which recognized the postsynaptic ACh receptors. Compared to the control mice, BTX-Rho labels revealed no obvious structural alteration in the NMJs of STX1B KO mice (Fig. 2*C*).

Deletion of STX1B in mice decreases the protein expression level of Munc18-1. Because Munc18-1 and Munc13-1 have been shown to have strong interactions with STX1 (Betz et al. 1997; Hata et al. 1993; Rizo and Rosenmund 2008), we then determined the protein expression levels of Munc18-1, Munc13-1, and other exo- and endocytic proteins in STX1B KO mice by Western blot (Fig. 3*A*). Quantification analysis revealed that the levels of STX1A, SNAP-25, SYB2, SYT1, SYN1, Munc13-1, and Rab5 were not significantly different between the control and KO brain lysates. However, a ~25% reduction of Munc18-1 level was observed in the STX1B KO brain lysate compared to the WT brain lysate (Fig. 3*B*). These data were consistent with previous findings that disruption of STX1 expression resulted in a reduction of Munc18-1 and indicated that STX1 and Munc18-1 are functionally closely related (Arancillo et al. 2013; Gerber et al. 2008; Zhou et al. 2013).

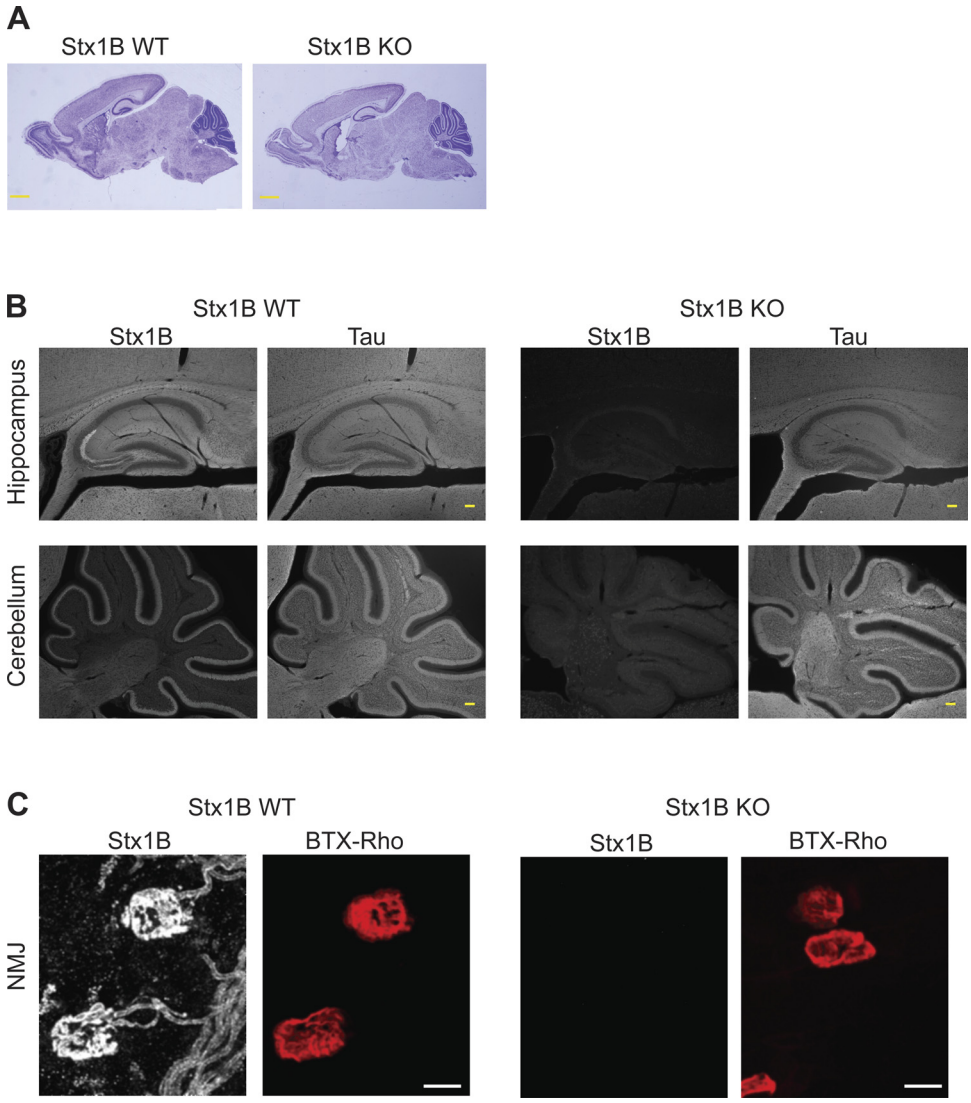

Fig. 2. Deletion of STX1B does not affect the brain gross morphology and the mouse neuromuscular junctions (NMJs). *A*: Nissl staining of brain slices from STX1B WT and KO mice at P10 suggested that STX1B KO mice were able to form proper brain morphology ($n = 3$ for each genotype). Scale bar, 1 mm. *B*: immunohistochemistry images of the hippocampus and cerebellum in the brain slices from STX1B WT and KO mice with antibodies recognizing STX1B and axonal marker Tau. Brain slices were prepared from animals at P10. Scale bar, 100 μm. *C*: micrographs of the NMJs from transversus abdominis (TVA) muscles from STX1B WT and KO mice at P8. Antibody recognizing STX1B identified the presynaptic terminals, whereas α-bungarotoxin conjugated to rhodamine (BTX-Rho) was used to label the postsynaptic ACh receptors. Scale bar, 10 μm.

Removal of STX1B does not alter synaptic transmission in autaptic hippocampal excitatory neurons and striatal inhibitory neurons. Since STX1 is a major component of the neuronal SNARE complex and the complex has an essential role in the neurotransmission, we first examined whether the loss of STX1B impairs the neurotransmitter release in hippocampal excitatory neurons and striatal inhibitory neurons. We took advantage of whole cell voltage-clamp recordings from autaptic culture system because it allows us to study the neurotransmission at a single-cell level (Bekkers and Stevens 1991).

Studies on autaptic hippocampal excitatory neurons revealed similar degrees of neurotransmission among the genotypes. Mean EPSC (Fig. 4*B*), mean RRP size assessed by 500 mM sucrose application, and mean P_{vr} determined by the evoked EPSC charge over the RRP charge in individual cells (Fig. 4*D*) all appeared similar among STX1B WT, Het, and KO neurons. Average spontaneous release (mEPSC) amplitudes and frequencies of the examined neurons were not significantly different among STX1B WT, Het, and KO neurons (Fig. 4*F*).

Neurotransmission examined in autaptic striatal inhibitory neurons also did not show significant differences among the genotypes. Mean evoked IPSC (Fig. 4*H*), mean RRP size, and mean P_{vr} (Fig. 4*J*) were all comparable among STX1B WT, Het, and KO neurons. Average spontaneous release (mIPSC) amplitudes and frequencies of the examined neurons also did not exhibit statistically significant differences among STX1B WT, Het, and KO cultures (Fig. 4*L*). These experiments indicate that STX1A functionally compensates for the loss of STX1B in recorded hippocampal excitatory and striatal inhibitory neurons.

High-density dissociated cerebellar cultures from STX1B KO mice had lower number of inhibitory neurons. Immunostaining results from P10 WT brain slices showed STX1B is strongly expressed at the molecular layer of the cerebellum (Fig. 2*B*), suggesting that STX1B may have an important role in cerebellar function. Therefore, we prepared high-density dissociated primary cerebellar cultures, which contained both excitatory granule cells and inhibitory neurons. We performed whole cell voltage-clamp recordings from cerebellar neurons, which were likely inhibitory neurons based on their cell morphology and the higher whole cell capacitance (>10 pF), and recorded pharmacologically isolated spontaneous synaptic currents in the presence of TTX. Analysis of mEPSC amplitudes

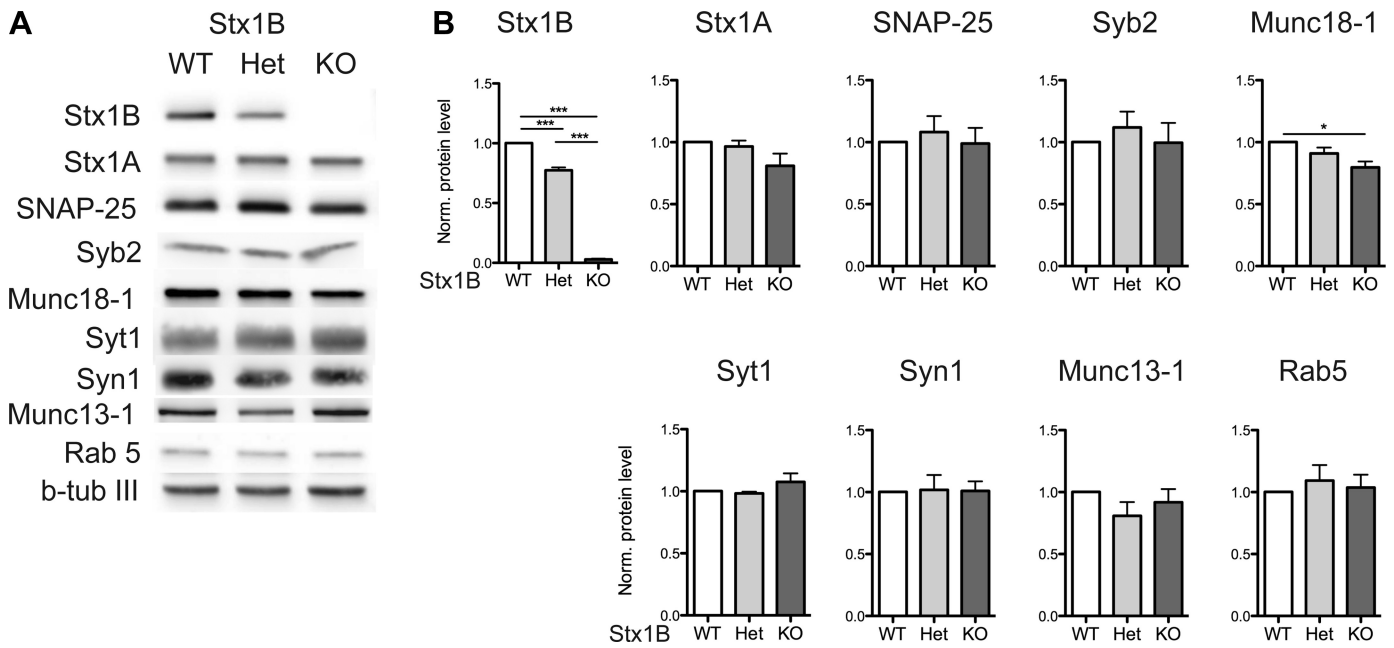

Fig. 3. Removal of STX1B in mice results in reduction of Munc18-1. *A*: Western blot analysis from the whole brain lysates from P10 to P11 animals showed the expression levels of STX1B, STX1A, synaptosomal-associated protein 25 (SNAP-25), synaptobrevin-2 (SYB2), Munc18-1, synaptotagmin-1 (SYT1), synaptophysin-1 (SYN1), Munc13-1, Rab5, and β-tubulin III (b-tub III). β-Tubulin III was used as an internal control. *B*: quantification of the protein expression levels from the Western blot ($n = 3$ for all of the proteins analyzed). The value of each protein was normalized (Norm.) to that of β-tubulin III in individual genotype in individual blot and then normalized to the WT ratio. Bar graphs show means ± SE. $*P \leq 0.05$; $***P \leq 0.001$.

and frequencies showed no significant differences among STX1B WT, Het, and KO cultures (Fig. 5*B*). To our surprise, we observed that the average mIPSC frequency was significantly reduced (approximately 50–60% reduction) and the average mIPSC amplitude was ~25% increased in cultures derived from STX1B KO mice (Fig. 5*D*).

Based on the electrophysiology results, we hypothesized two possible causes for the reduction of the average mIPSC frequency in STX1B KO cultures. First, it has been demonstrated that a reduction of STX1 protein levels results in a decrease in vesicle fusogenicity (Arancillo et al. 2013). For this reason, if STX1B is the predominate isoform in cerebellar inhibitory cells, we would expect that vesicle fusogenicity is impaired. Second, studies have also shown that loss of both STX1A and STX1B in hippocampal as well as in cortical neurons resulted in cell death in vivo and in vitro (Mishima et al. 2014; G. Vardar and C. Rosenmund, unpublished observations). Therefore, if STX1B is the major isoform in cerebellar inhibitory cells, loss of STX1B would lead to cell death and consequently to fewer synapses in dissociated cultures.

To test the first hypothesis, we applied different concentrations (150, 250, and 500 mM) of the sucrose solution to each cell during the recording. The response to each sucrose application was normalized to the RRP size evoked by 500 mM sucrose within individual cells to determine the fraction of the released pool. Each normalized response was integrated, and then the maximal slope was quantified as the peak release rate (Basu et al. 2007). In a comparison among STX1B WT, Het, and KO neurons, the peak release rate at respective concentration of sucrose was very similar (Fig. 5*E*). Therefore, the decrease in mIPSC frequency in STX1B KO cerebellar cultures was unlikely due to a decrease in fusogenicity caused by fewer copy numbers of STX1.

To address the second hypothesis, high-density dissociated cerebellar cultures were immunostained with the NeuN, VGlut1, and VGAT antibodies and imaged at a low magnification (Fig. 5*F*). The average neuron number (NeuN-positive cells) in the field of view in STX1B KO cultures was ~27% lower than that in the WT and Het cultures (Fig. 5*G*). The density of VGlut1-positive puncta per 0.15 mm^2 was similar among STX1B WT, Het, and KO cultures, yet the density of VGAT-positive puncta per 0.15 mm^2 was significantly lower in the STX1B KO cultures (~25% reduction; Fig. 5*G*). Taken together, depletion of STX1B resulted in an enhanced loss of inhibitory neurons in the cerebellar cultures, which was accompanied by a reduction of inhibitory synapses and mIPSC frequencies in the dissociated cerebellar culture.

Neurotransmission is affected in the motor nerve terminals of STX1B KO mice. Based on the observation that STX1B KO mice showed motor abnormalities and the prominent expression of STX1B at the TVA terminals (Fig. 2*C*), we explored whether the absence of STX1B affected neurotransmission in motor nerve terminals. TVA muscles were prepared from STX1B WT, Het, and KO mice at P8 (mouse number, WT: $N = 5$; Het: $N = 4$; KO: $N = 3$), and intracellular recordings were performed from these muscle fibers.

The analysis of the spontaneous release revealed no change in the mean frequency among the different genotypes (Fig. 6*A*) but a right shift in the curve representing mEPP amplitude versus cumulative fraction of events in STX1B KO NMJs with respect to WT and Het NMJs (Fig. 6*B*). Similarly, a significant increase in the mean mEPP amplitude in STX1B KO (~129%) was found compared with STX1B WT (Fig. 6*C*). Moreover, evoked synaptic transmission activity showed a reduction in the NMJs from the STX1B KO mice. Mean EPP amplitude was smaller in the STX1B KO muscles compared with the

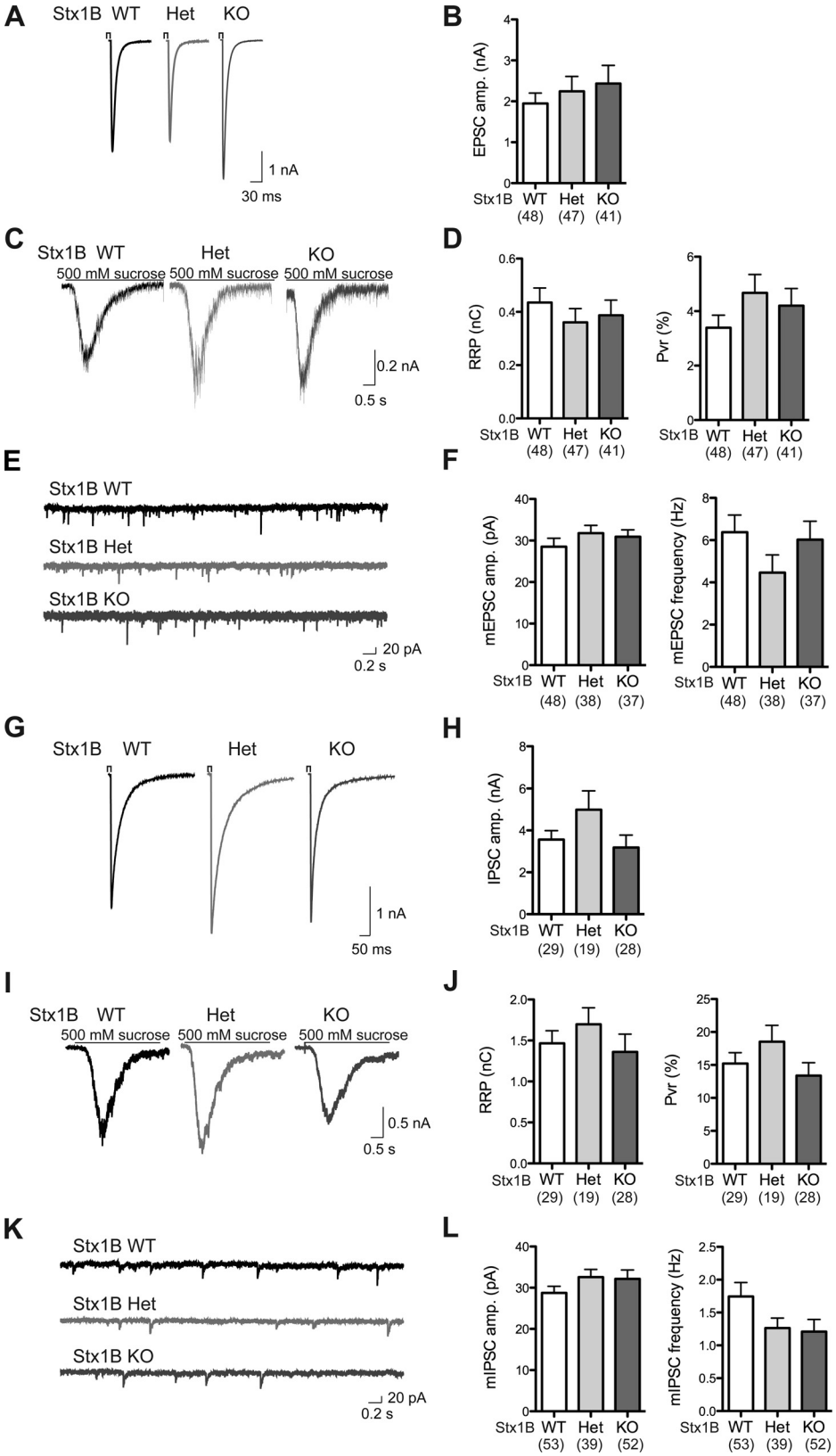

Fig. 4. Hippocampal excitatory neurons and striatal inhibitory neurons show normal synaptic transmission in the absence of STX1B. *A*: sample traces of excitatory postsynaptic current (EPSC) from STX1B WT (black), Het (light gray), and KO (dark gray) neurons after a 2-ms depolarization. *B*: plot of average EPSC amplitudes (amp.) in STX1B WT, Het, and KO autaptic hippocampal excitatory neurons. *C*: sample traces of responses from STX1B WT (black), Het (light gray), and KO (dark gray) hippocampal excitatory neurons during 500 mM sucrose application for 5 s. *D*: plots of average readily releasable pool (RRP) size and vesicular release probability (P_{vr}) in STX1B WT, Het, and KO autaptic hippocampal excitatory neurons. *E*: sample traces of mEPSC from STX1B WT (black), Het (light gray), and KO (dark gray) neurons. *F*: plots of mean mEPSC amplitudes and frequencies are presented. *G*: sample traces of inhibitory postsynaptic current (IPSC) from STX1B WT (black), Het (light gray), and KO (dark gray) neurons after a 2-ms depolarization. *H*: average IPSC amplitudes in STX1B WT, Het, and KO autaptic striatal inhibitory neurons are shown. *I*: sample traces of responses from STX1B WT (black), Het (light gray), and KO (dark gray) striatal inhibitory neurons during 500 mM sucrose application for 5 s. *J*: plots of average RRP size and P_{vr} in autaptic striatal inhibitory neurons from STX1B WT, Het, and KO cultures. *K*: sample traces of mIPSC from STX1B WT (black), Het (light gray), and KO (dark gray) neurons. *L*: mean mIPSC amplitudes and frequencies are presented. All bar graphs are presented with means ± SE. The total number of neurons examined in each genotype is indicated in the graphs.

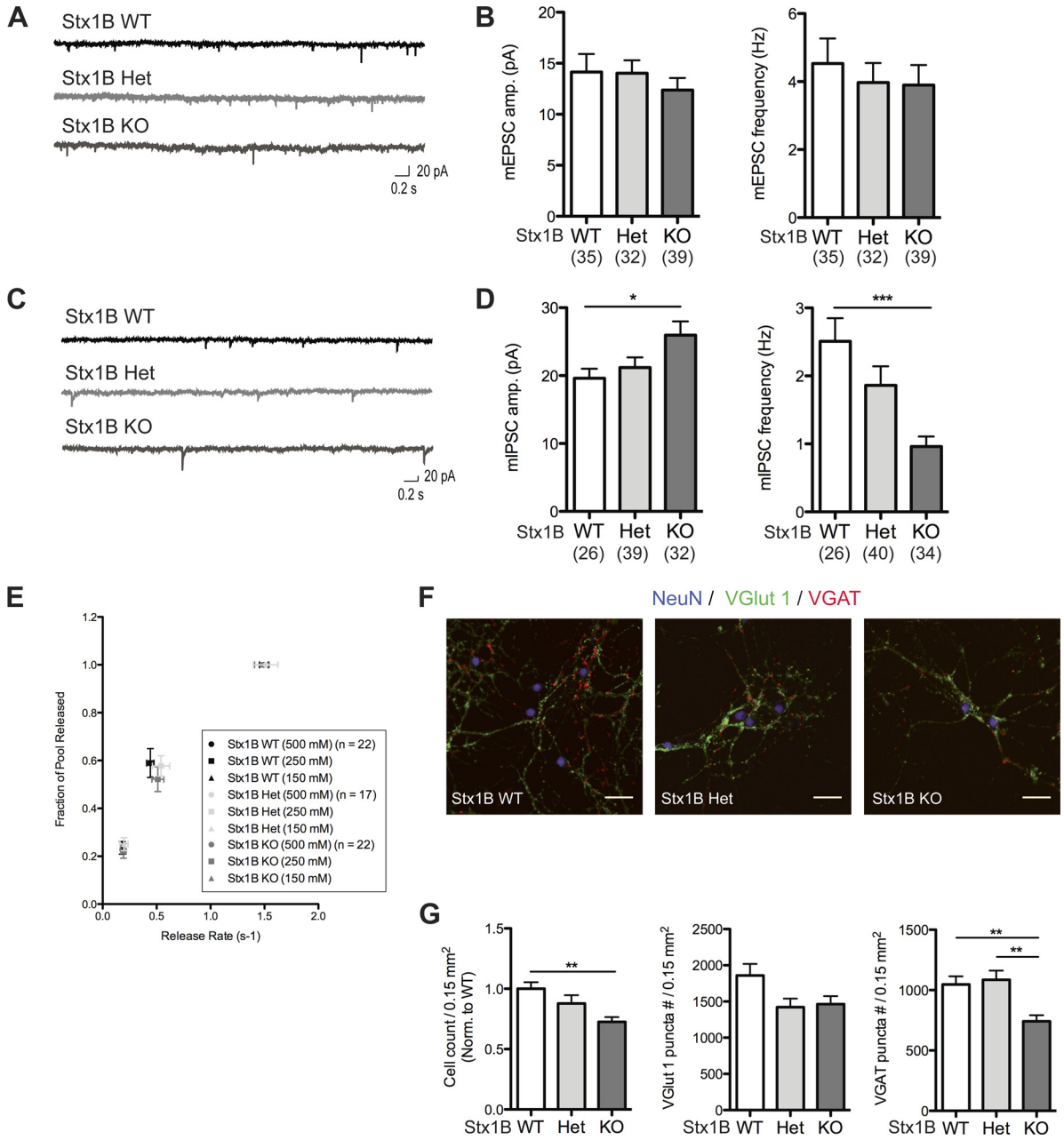

Fig. 5. Deletion of STX1B from mice causes a reduction of GABAergic transmission in high-density dissociated cerebellar cultures. *A*: sample traces of mEPSC input on STX1B WT (black), Het (light gray), and KO (dark gray) neurons. *B*: plots showing mean mEPSC amplitudes and frequencies in high-density cerebellar cultures. *C*: sample traces of mIPSC input on STX1B WT (black), Het (light gray), and KO (dark gray) neurons. *D*: plots showing average mIPSC amplitudes and frequencies in high-density cerebellar cultures. Bar graphs in *B* and *D* show means ± SE. $*P \leq 0.05$; $***P \leq 0.001$. The number of neurons examined in each condition is indicated in the graphs. *E*: summary plot of the fraction of RRP and its corresponding peak release rate. Data were collected from the 3 genotypes (STX1B WT: black, $n = 22$; STX1B Het: light gray, $n = 17$; STX1B KO: dark gray, $n = 22$) at 500 mM (circle), 250 mM (square), and 150 mM (triangle) sucrose applications. All sucrose responses were normalized to the RRP size (500 mM sucrose response) to determine the fraction of the pool released. *F*: example images of cerebellar cultures from STX1B WT, Het, and KO cultures. Antibodies recognizing NeuN (blue), vesicular glutamate transporter 1 (VGlut1; green), and vesicular GABA transporter (VGAT; red) were used to quantify the neuronal number and the density of excitatory and inhibitory synapses, respectively. Scale bar, 20 μm. *G*: bar graphs with means ± SE illustrating neuronal number and the mean density of VGlut1 and VGAT puncta per 0.15 mm^2. Neuronal number obtained from each genotype was normalized to that from the STX1B WT cultures (STX1B WT: $n = 34$ images; STX1B Het: $n = 35$ images; STX1B KO: $n = 36$ images; with 4 cultures). Densities of VGlut1 puncta and VGAT were obtained from 47 images for STX1B WT, 47 images for STX1B Het, and 48 images for STX1B KO (with 5 cultures). $**P \leq 0.01$.

WT and Het muscles (~25% smaller than WT and ~41% smaller than Het; Fig. 6*E*). Therefore, the number of vesicles released per action potential (quantal content; calculated as the mean evoked EPP amplitude divided by the mean mEPP amplitude in individual muscle fibers) revealed a significant reduction of release in STX1B KO mice compared to WT and Het ones (~36% reduction; Fig. 6*F*).

Additionally, the input resistance of the muscle fibers was ~248% higher for STX1B KO mice compared to STX1B

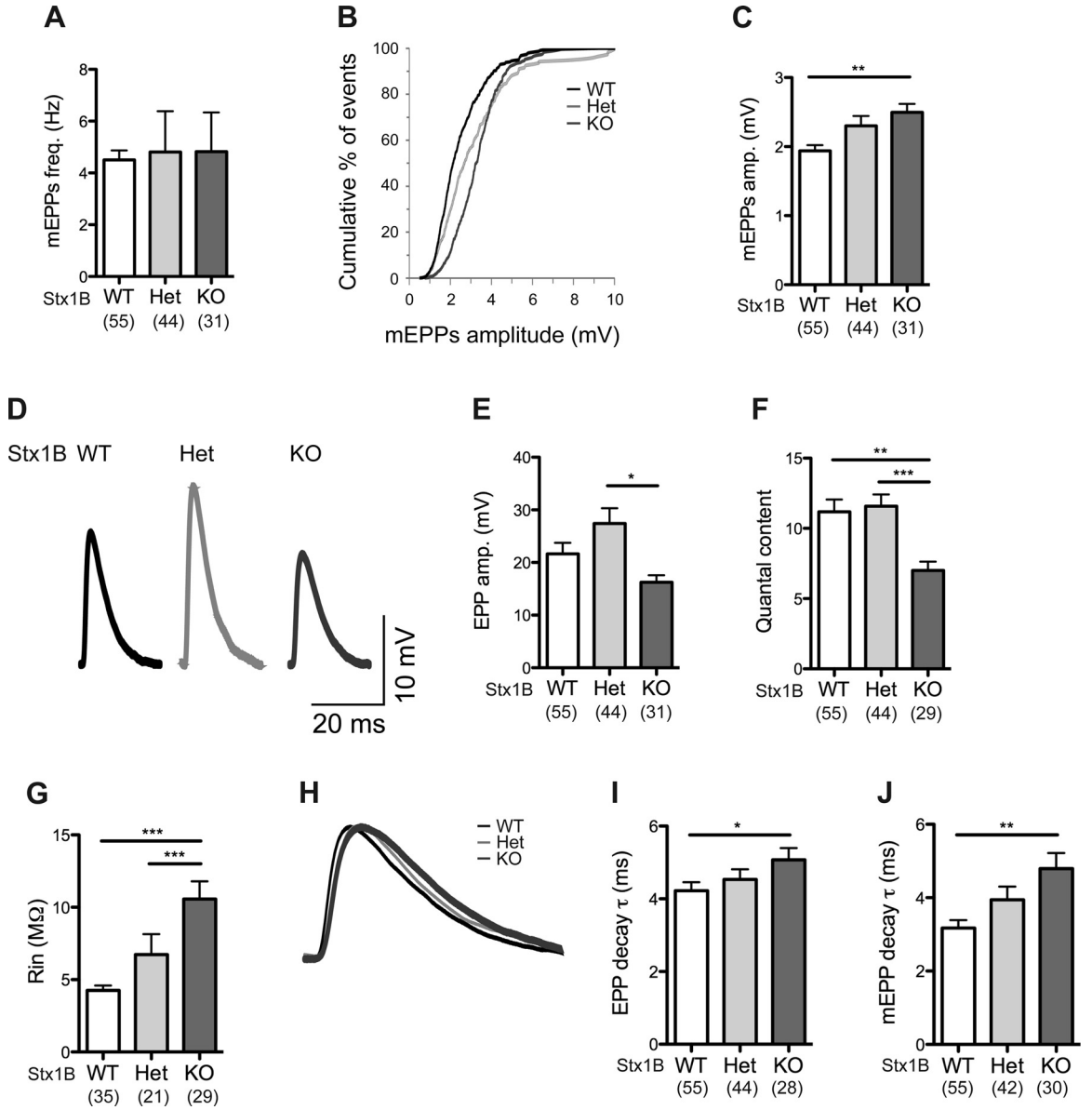

Fig. 6. STX1B is important to support a normal neurotransmission at the mouse NMJs. *A*: frequencies of mean miniature end-plate potentials (mEPPs freq.) from STX1B WT (white), Het (light gray), and KO (dark gray). *B*: cumulative fraction of mEPP amplitudes in STX1B WT (black), Het (light gray), and KO (dark gray). *C*: bar graph showing amplitudes of mean mEPPs in STX1B WT, Het, and KO NMJs. *D*: representative EPP traces from STX1B WT (black), Het (light gray), and KO (dark gray) NMJs. *E* and *F*: mean EPP amplitudes (*E*) and quantal content (*F*) among the 3 genotypes. *G*: bar graph showing mean input resistance (R_{in}) of the muscle fibers from STX1B WT (white), Het (light gray), and KO (dark gray) mice. *H*: amplitude-normalized EPP traces in STX1B WT (black), Het (light gray), and KO (dark gray) fibers. *I* and *J*: decay time constant (τ) of EPPs and mEPPs, respectively, in STX1B WT (white), Het (light gray), and KO (dark gray) muscle fibers. All bar graphs show means ± SE. The number of muscle fibers examined in each genotype is indicated in the graph. $*P \leq 0.05$; $**P \leq 0.01$; $***P \leq 0.001$.

WT mice (Fig. 6*G*), suggesting that the muscle fibers are smaller in STX1B KO mice. This result corresponds to the increased mEPP amplitudes in STX1B KO NMJs (Fig. 6*C*) as well as the slower kinetics of the EPP and mEPP waveforms (~120 and ~151%, respectively, longer decay time constant for KO compared to WT and Het) for STX1B KO mice (Fig. 6, *I* and *J*).

The motor nerve terminals of STX1B KO mice show a higher degree of depression. To investigate further the impact of STX1B on neurotransmission at the TVA muscle fibers, we examined the short-term synaptic plasticity with a stimulus train (20 Hz, 5 s). During the initial part of the train stimulation, a small degree of facilitation was observed in all cases. After the facilitation, the responses decreased with an exponential decline, known as short-term depression (Fig. 7, *A* and *B*). An increased synaptic depression was observed in STX1B KO TVA muscle fibers (Fig. 7*C*). As a result, the release ratio (determined by the mean responses of the last 50 pulses over the 1st response) was also significantly reduced in STX1B KO TVA muscle fibers compared to WT and Het TVA ones (~30% reduction; Fig. 7*D*). Moreover, since the absence of STX1B did not completely abolish neurotransmission at TVA muscles, we speculated that STX1A may be compensating for the function as has been shown in the synapses at the CNS. Indeed, we could detect STX1A by immunostaining in the NMJs prepared from STX1B KO mice (Fig. 7*E*), suggesting that the

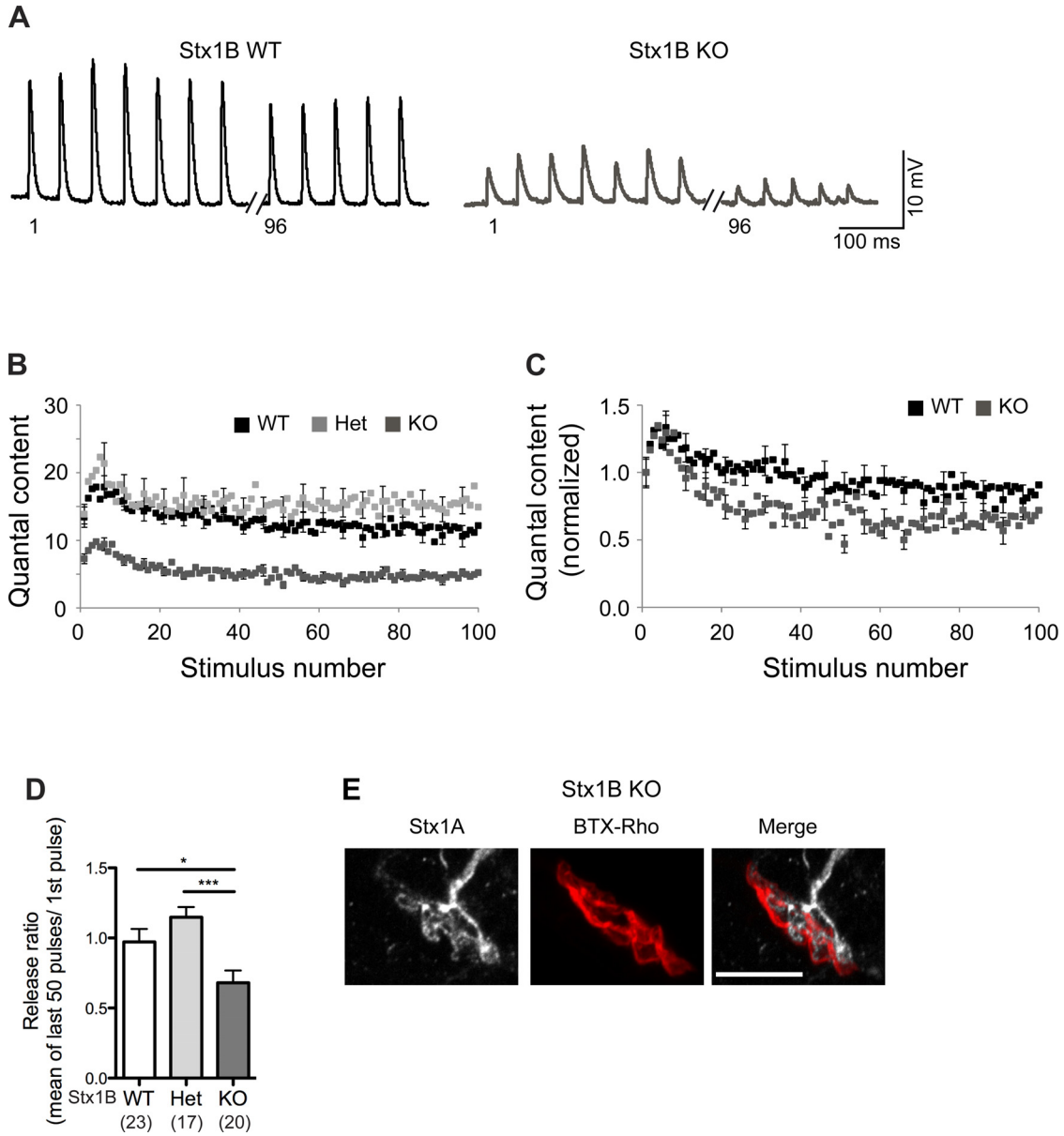

Fig. 7. Motor nerve terminals in STX1B KO mice present more short-term depression than those in the control mice. *A*: sample traces showing EPP responses at the 1st 7 stimuli and at the last 5 stimuli of a 20-Hz train (5 s) in STX1B WT (black) and KO (dark gray) NMJs. *B* and *C*: mean and normalized, respectively, quantal content during the train of stimulation in STX1B WT (black), Het (light gray), and KO (dark gray). *D*: bar graphs showing the release ratio (determined by the average responses of the last 50 stimuli divided by the 1st response) from the 3 genotypes. *E*: *z*-stack projections of motor nerve terminals from TVA muscle from STX1B KO mice stained with BTX-Rho (red) and anti-STX1A antibody (white). Scale bar, 10 μm. $*P \leq 0.05$; $***P \leq 0.001$.

residual responses observed in STX1B KO motor nerve terminals is most likely due to a partial redundancy of STX1A.

Selective removal of STX1B from forebrain excitatory neurons also affects mouse postnatal survival. The abundant expression pattern of STX1B in the CNS prompted us to wonder whether region-specific deletion of STX1B in mice would also result in postnatal development deficiency. Therefore, we generated a STX1B FL mouse line ($STX1B^{FL/FL}$) by crossing mice harboring the targeted locus with ROSA-FLP deleter mice to remove the FRT-flanked neomycin cassette (Farley et al. 2000; Fig. 8*A* and MATERIALS AND METHODS). $STX1B^{FL/FL}$ mice were further crossed to CamKIIα-Cre mice (Casanova et al. 2001) to obtain a selective deletion of STX1B from forebrain excitatory neurons ($STX1B^{FL/FL}$;$CamK^{Cre/+}$). Western blot of the total brain lysates collected from $STX1B^{FL/FL}$;$CamK^{Cre/+}$ mice at P15 showed a drastic decrease in the STX1B protein level compared to the brain lysate from the control littermate ($STX1B^{FL/FL}$;$CamK^{+/+}$; Fig. 8*B*). The growth curve revealed that $STX1B^{FL/FL}$;$CamK^{Cre/+}$ mice had weight comparable with their control littermates at the 1st postnatal week but started to lose weight around P10 (Fig. 8*C*). The survival curve showed that although they survived longer than STX1B KO mice, $STX1B^{FL/FL}$;$CamK^{Cre/+}$ mice eventually also succumbed to death before P19 (Fig. 8*D*). Interestingly, our growth and survival curves showed a similar trend to the expression of CamKIIα promoter-driven Cre, which has been shown to start around P3 and reached the maximum level at P15 (Casanova et al. 2001). We further explored whether these conditional KO

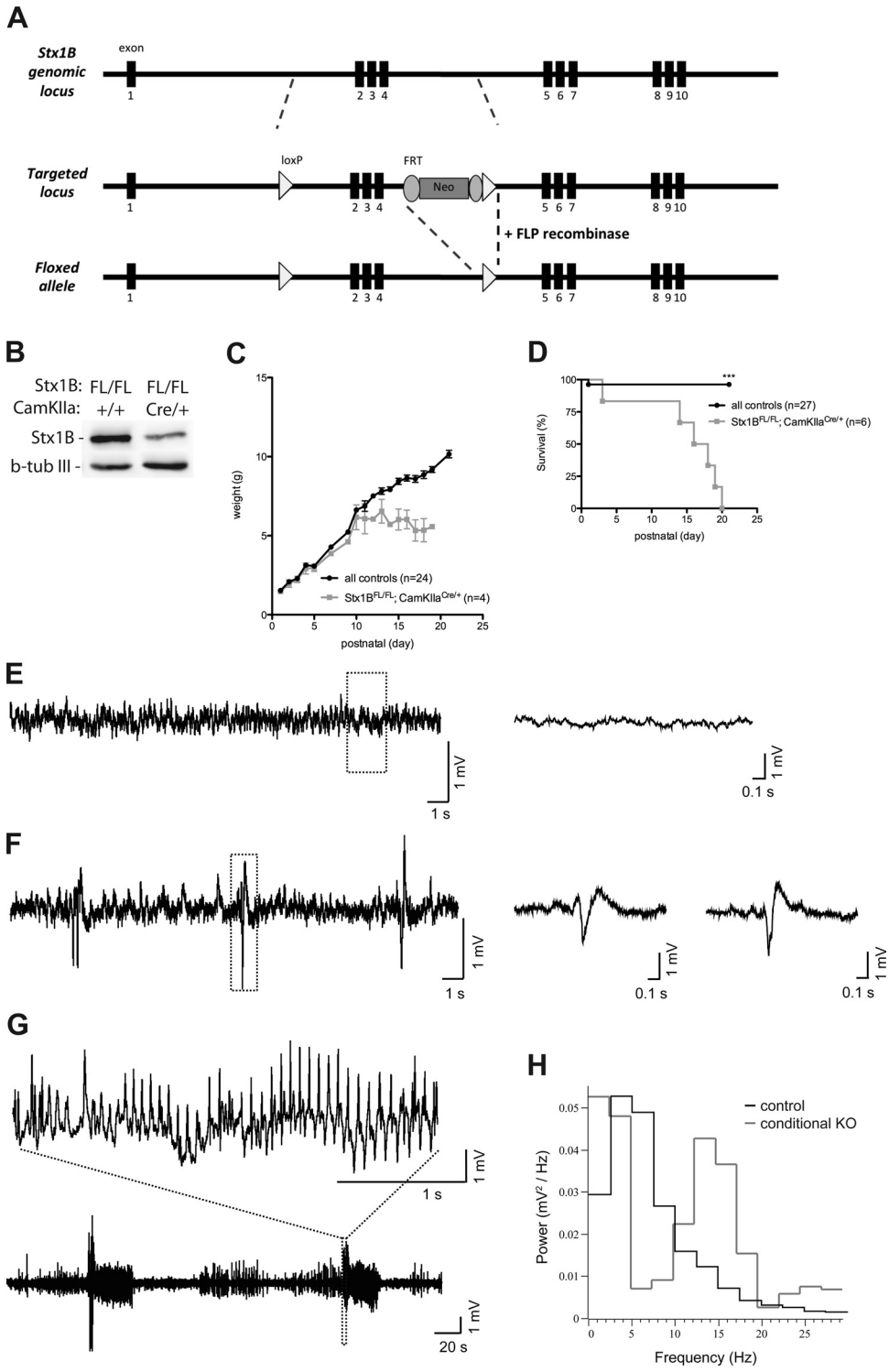

Fig. 8. Deletion of STX1B from the mouse forebrain excitatory neurons also results in premature death and hypersynchronous brain activity. *A*: cloning strategy for the generation of mice carrying floxed (FL) STX1B alleles ($STX1B^{FL/FL}$). *B*: Western blot analysis from the whole brain lysates from mice at P15. The protein expression level of STX1B was reduced in the $STX1B^{FL/FL}$;$CamKII\alpha^{Cre/+}$ brain lysate compared with the $STX1B^{FL/FL}$;$CamKII\alpha^{+/+}$ brain lysate. β-Tubulin III was used as an internal control. *C*: growth curve of control and $STX1B^{FL/FL}$;$CamKII\alpha^{Cre/+}$ mice showing that $STX1B^{FL/FL}$;$CamKII\alpha^{Cre/+}$ mice stopped gaining weight from P10 on. *n*, Number of animals monitored. *D*: survival curve showing that all monitored $STX1B^{FL/FL}$;$CamKII\alpha^{Cre/+}$ mice succumbed to death before P20. During the observation period, 1 control pup ($STX1B^{+/+}$;$CamKII\alpha^{Cre/+}$) also died at P1. Number of animals monitored for each genotype was indicated in the graph. ***$P \leq 0.001$. *E–G*: examples of cortical EEG recorded in freely moving conditional KO and control mice. Control mice ($n = 6$) exhibited normal EEG (*E*), whereas $STX1B^{FL/FL}$;$CamKII\alpha^{Cre/+}$ mice ($n = 6$) displayed a hypersynchronous EEG with interictal (*F*) and ictal (*G*) activity. Representative traces are continuous recordings from an EEG channel taken from prolonged monitoring of each mouse. The ictal pattern was characterized by bursts of spike-wave complexes. During 2-h recording, this mouse exhibited 8 episodes of such bursts, each of which lasted between 28 and 45 s, and multiple interictal spikes. The boxed regions in traces on the *left* are amplified on the *right* (*E* and *F*) or *top* (*G*). *G* and *H*: power spectrum of the recording epochs shown in *E* control mouse, black line (*H*), and conditional KO mouse, dark gray line (*G*). The control spectrum is scaled by the ratio of conditional KO-to-control maximal power. Note the power peak in the conditional KO at ~15 Hz.

mice exhibited any abnormal brain activity. Cortical EEG was recorded on P15–P16 mice. Control animals ($STX1B^{+/+}$; $CamK^{Cre/+}$ and $STX1B^{FL/FL}$;$CamK^{+/+}$, $n = 6$) did not display pathological electrographic activity or motor seizures (Fig. 8*E*). EEG of the $STX1B^{+/+}$;$CamK^{Cre/+}$ mice showed interictal and ictal EEG activity in five out of six recorded mice (Fig. 8, *F* and *G*). Interictal activity consisted of intermittent population spikes (Fig. 8*F*). In contrast to the control mice, the ictal EEG patterns (characteristic for epileptiform activity) from $STX1B^{FL/FL}$;$CamK^{Cre/+}$ mice featured a rapid voltage deflection followed by regular high-amplitude activity that developed into polyspike bursts at ~15 Hz (Fig. 8, *G* and *H*). In three $STX1B^{FL/FL}$;$CamK^{Cre/+}$ mice, this activity was accompanied by motor focal clonic seizures. These data support that STX1B is essential for postnatal survival and may imply that the function of STX1B in neurotransmission in certain neurons in the forebrain cannot be compensated. However, precise mechanisms still remain to be clarified.

DISCUSSION

STX1 is the main neuronal syntaxin that is critical for synaptic transmission (Saifee et al. 1998; Schulze et al. 1995). Mammalian STX1 includes two highly similar paralogs, STX1A and STX1B, which have been reported to express abundantly throughout neuronal tissues in rodents (Aguado et al. 1999; Ruiz-Montasell et al. 1996) and are believed to have functional redundancy (Arancillo et al. 2013; Bennett et al. 1992). In the current study, we wanted to address whether STX1B has a differential role from STX1A by investigating autaptic hippocampal glutamatergic and autaptic striatal GABAergic neuronal cultures, high-density dissociated cerebellar cultures, and NMJs from STX1B KO mice. Our major findings are as follows. *1*) In contrast to STX1A KO mice (Fujiwara et al. 2006), complete knockout of STX1B or selective removal of it from forebrain excitatory neurons resulted in a premature death of mice, suggesting that STX1B is an essential protein for postnatal survival (Figs. 1 and 8). *2*) High-density cerebellar neuronal cultures derived from STX1B KO mice have a lower amount of cell number, implying that STX1B is also important for neuronal survival in vitro (Fig. 5). *3*) Deletion of STX1B in mice decreases the efficiency of the neurotransmission at the NMJs and reduces the size of the muscle fibers (Figs. 6 and 7).

In line with earlier studies (Arancillo et al. 2013; Fujiwara et al. 2006; Gerber et al. 2008), we also demonstrated that deletion of a single STX1 paralog alone in mice is not sufficient to impair neurotransmission in autaptic hippocampal excitatory neurons or autaptic striatal inhibitory neurons (Fig. 4), indicating that STX1A and STX1B are functionally redundant in these cell types. Interestingly, similar to the reduced mEPSC and mIPSC frequencies reported recently by Mishima et al. (2014), we also detected lower spontaneous GABAergic transmission frequencies in high-density cerebellar cultures (Fig. 5). Moreover, a recent study has linked STX1B to the fever-associated seizure activities in children and zebrafish. In this report, zebrafish larvae with knockdown STX1B developed abnormal brain activities when the temperature was increased, and this phenotype could be rescued with WT STX1B but not with mutated STX1B, implying a possible differential role of STX1B from STX1A in neurotransmission (Schubert et al. 2014). However, we performed our experiments at room temperature, and, therefore, we favor the interpretation that the downscaling of mIPSC frequencies detected in the high-density neuronal cultures is due to a lower number of neurons and inhibitory synapses in the STX1B KO cerebellar cultures (Fig. 5). These results would support the idea that STX1B is essential for the neuronal survival and argue against impairment of the neurotransmission machinery induced by removing only STX1B in these neurons. For this reason, we did not observe significant differences in synaptic function in autaptic neuronal cultures derived from STX1B KO mice.

Indeed, unlike other neuronal SNARE proteins, mouse cortical and hippocampal neurons in the absence of both STX1 paralogs undergo cell death in vitro (Mishima et al. 2014; G. Vardar and C. Rosenmund, unpublished observations). Since STX1 is an abundant plasma membrane protein, in addition to its function in neurotransmission, STX1 has been proposed to be important for retaining essential plasma membrane recycling processes, without which cellular degeneration may occur (Peng et al. 2013). In a recent study, Kofuji et al. (2014) have reported a decreased number of NeuN-positive cells in the hippocampus of STX1B KO mice at P7 imaged at a high magnification. The authors also showed that hippocampal neurons derived from STX1B KO mice had lower cell viability compared with those from WT and STX1A KO mice when growing on poly-L-lysine-coated glass coverslips. The cell viability for STX1B KO hippocampal neurons in vitro could be restored when neurons were grown on WT or STX1A KO glial cells but not on STX1B KO glial cells (Kofuji et al. 2014). In our study, we grew neurons on WT glial cells, yet the cell viability for STX1B KO cerebellar neurons was still lower than control neurons in vitro (Fig. 5). Hence, we hypothesize that certain types of neurons may express only or predominantly STX1B, and when STX1B is genetically deleted, these neurons tend to undergo cell death. However, which hippocampal and cerebellar neurons are affected remain to be identified.

Furthermore, we have also investigated the function of STX1B at the mouse NMJs and provided an important insight for the first time into the involvement of STX1B in synaptic transmission at the mouse PNS. In our study, we found that deletion of STX1B in mice caused an increased mean mEPP amplitude and changes in the mEPP and EPP waveform kinetics (Fig. 6), and these phenotypes could be correlated to smaller muscle fibers in the STX1B KO mice (higher input resistant of the muscle fibers; Fig. 6). Despite a smaller size of the muscle fibers, the maturation of the endplate was unaltered, suggesting that STX1B is dispensable for the formation of the mouse NMJs (Fig. 2). In contrast to the normal synaptic transmission in neurons examined in the autaptic cultures from the CNS, there was ~40% reduction in the neurotransmitter release at the NMJs from STX1B KO mice. One plausible explanation for the incomplete reduction in neurotransmission is that the presence of STX1A could support only a partial function at the mouse NMJs (Fig. 7; Aguado et al. 1999). Moreover, we also observed that despite a similar degree of the initial facilitation, STX1B KO NMJs displayed a more depressed plateau than the WT and Het NMJs during high-frequency stimulation (Fig. 7). Interestingly, a similar phenotype was also described in the mouse Munc18-1 Het NMJs (Toonen et al. 2006). These data once again signify that the STX1-Munc18-1 dimer works closely to maintain the function of neurotransmitter release and to sustain synaptic efficiency (Mitchell and Ryan 2005; Rizo and Südhof 2012).

SNAP-25 and SYB1 (a paralog of SYB2 in mice) have also been implied to be important for the neurotransmission at the mouse NMJs. However, it is interesting to note that deletion of these SNARE proteins individually in mice results in different phenotypes. Analysis of diaphragm muscle fibers from SNAP-25 KO mice at *embryonic day 17.5-18.5* revealed a decreased number of diaphragm muscle fibers and less organized synaptic staining patterns. Whereas the evoked transmission is completely abolished in SNAP-25 KO NMJs, the average spontaneous release frequency appeared to be normal and the mean spontaneous transmission amplitude is twofold larger in SNAP-25 KO NMJs compared to the controls (Washbourne et al. 2002). Although more direct evidence still needs to be provided, it has been suggested that another paralog, for example SNAP-23, might partially replace SNAP-25 at the mouse NMJs (Sørensen et al. 2003; Varoqueaux et al. 2005). Additionally, similar to STX1B KO mice, SYB1 KO mice

were viable at birth but also exhibited motor impairment during the 1st postnatal week and a preweaning death (Nystuen et al. 2007). The structures of the NMJs of diaphragm muscles in SYB1 KO mice were also comparable with those in the control mice. However, mean evoked amplitudes and spontaneous transmission frequencies were only partially decreased in SYB1 KO mouse NMJs (~40% and ~60% reduction, respectively), and this was most likely due to the presence of SYB2 (Liu et al. 2011). Although the reason of the death for SYB1 KO mice was probably due to insufficient EPPs to elicit muscle contractions for normal body functions such as breathing activity (Liu et al. 2011), the reason of the premature death for STX1B KO mice may be more complicated. We have noticed that the STX1B KO mice had a much smaller size and much lighter weight compared to the control littermates (Figs. 1 and 8), suggesting that STX1B KO mice may also have defects in food uptake and/or growth signaling. However, the precise causes for the death to STX1B KO mice remain to be studied.

In conclusion, by analyzing excitatory neurons and inhibitory neurons from several regions in the CNS and the TVA NMJs in STX1B KO mice, we could demonstrate that STX1B is essential for the survival of neurons in vitro and it is a critical syntaxin protein for the neurotransmission at the mouse NMJs. To our knowledge, our study shows for the first time that STX1B is dispensable for the formation of the mouse NMJs but it is required for maintaining the proper neurotransmission at the mouse NMJs. The importance of STX1B in the neurotransmission at the mouse NMJ and likely also in the cerebellar circuits may contribute to the motor defects that occurred in STX1B KO mice and mice with a lower level of STX1B (Arancillo et al. 2013; Gerber et al. 2008; Kofuji et al. 2014). Furthermore, although STX1A and STX1B are highly homologous and functionally redundant, subtle differences between them, such as location or expression level, could explain the apparent differences in the respective KO mice.

ACKNOWLEDGMENTS

We thank Bettina Brokowski, Annegret Felies, Sabine Lenz, Katja Poetschke, and Berit Soehl-Kielczynski for their excellent technical assistance; Marcial Camacho-Perez and Melissa Herman for comments on the manuscript; and members of the Rosenmund laboratory for discussions.

Present address of Y.-J. Wu: Pasteur Institute, Unit of Membrane Traffic and Pathogenesis, 75724 Paris Cedex 15, France.

Present address of M. Arancillo: Dept. of Pathology and Immunology and Dept. of Neuroscience, Baylor College of Medicine, Jan and Dan Duncan Neurological Research Institute of Texas Children's Hospital, Houston, TX 77030.

GRANTS

This study was supported by the Excellence Cluster NeuroCure Exc257 (to C. Rosenmund, T. Korotkova, and A. Ponomarenko) and the Spanish Ministry of Science and Innovation BFU2013-43763-P and BES2011-048901 (to L. Tabares and R. Tejero).

DISCLOSURES

No conflicts of interest, financial or otherwise, are declared by the author(s).

AUTHOR CONTRIBUTIONS

Y.-J.W., M.A., D.S., A.P., L.T., and C.R. conception and design of research; Y.-J.W., R.T., M.A., G.V., T.K., and M.K. performed experiments; Y.-J.W., R.T., M.A., and T.K. analyzed data; Y.-J.W., R.T., T.K., L.T., and C.R. interpreted results of experiments; Y.-J.W., R.T., and T.K. prepared figures; Y.-J.W., R.T., T.K., L.T., and C.R. drafted manuscript; Y.-J.W., R.T., G.V., L.T., and C.R. edited and revised manuscript; Y.-J.W., R.T., M.A., G.V., T.K., M.K., D.S., A.P., L.T., and C.R. approved final version of manuscript.

REFERENCES

Adams DJ, Quail MA, Cox T, van der Weyden L, Gorick BD, Gorick BD, Su Q, Chan WI, Davies R, Bonfield JK, Law F, Humphray S, Plumb B, Liu P, Rogers J, Bradley A. A genome-wide, end-sequenced 129Sv BAC library resource for targeting vector construction. *Genomics* 86: 753–758, 2005.

Aguado F, Majo G, Ruiz-Montasell B, Llorens J, Marsal J, Blasi J. Syntaxin 1A and 1B display distinct distribution patterns in the rat peripheral nervous system. *Neuroscience* 88: 437–446, 1999.

Arancillo M, Min SW, Gerber S, Münster-Wandowski A, Wu YJ, Herman M, Trimbuch T, Rah JC, Ahnert-Hilger G, Riedel D, Südhof TC, Rosenmund C. Titration of Syntaxin1 in mammalian synapses reveals multiple roles in vesicle docking, priming, and release probability. *J Neurosci* 33: 16698–16714, 2013.

Basu J, Betz A, Brose N, Rosenmund C. Munc13-1 C1 domain activation lowers the energy barrier for synaptic vesicle fusion. *J Neurosci* 27: 1200–1210, 2007.

Bekkers JM, Stevens CF. Excitatory and inhibitory autaptic currents in isolated hippocampal neurons maintained in cell culture. *Proc Natl Acad Sci USA* 88: 7834–7838, 1991.

Bennett MK, Calakos N, Scheller RH. Syntaxin: a synaptic protein implicated in docking of synaptic vesicles at presynaptic active zones. *Science* 257: 255–259, 1992.

Betz A, Okamoto M, Benseler F, Brose N. Direct interaction of the rat unc-13 homologue Munc13-1 with the N terminus of syntaxin. *J Biol Chem* 272: 2520–2526, 1997.

Bilimoria PM, Bonni A. Cultures of cerebellar granule neurons. *CSH Protoc* 2008: pdb.prot5107, 2008.

Casanova E, Fehsenfeld S, Mantamadiotis T, Lemberger T, Greiner E, Stewart AF, Schütz G. A CamKIIalpha iCre BAC allows brain-specific gene inactivation. *Genesis* 31: 37–42, 2001.

Deitcher DL, Ueda A, Stewart BA, Burgess RW, Kidokoro Y, Schwarz TL. Distinct requirements for evoked and spontaneous release of neurotransmitter are revealed by mutations in the *Drosophila* gene neuronal-synaptobrevin. *J Neurosci* 18: 2028–2039, 1998.

Facci L, Skaper SD. Culture of rat cerebellar granule neurons and application to identify neuroprotective agents. *Methods Mol Biol* 846: 23–37, 2012.

Farley FW, Soriano P, Steffen LS, Dymecki SM. Widespread recombinase expression using FLPeR (flipper) mice. *Genesis* 28: 106–110, 2000.

Fujiwara T, Mishima T, Kofuji T, Chiba T, Tanaka K, Yamamoto A, Akagawa K. Analysis of knock-out mice to determine the role of HPC-1/syntaxin 1A in expressing synaptic plasticity. *J Neurosci* 26: 5767–5776, 2006.

Gerber SH, Rah JC, Min SW, Liu X, de Wit H, Dulubova I, Meyer AC, Rizo J, Arancillo M, Hammer RE, Verhage M, Rosenmund C, Südhof TC. Conformational switch of syntaxin-1 controls synaptic vesicle fusion. *Science* 321: 1507–1510, 2008.

Hata Y, Slaughter CA, Südhof TC. Synaptic vesicle fusion complex contains unc-18 homologue bound to syntaxin. *Nature* 366: 347–351, 1993.

Hong W, Lev S. Tethering the assembly of SNARE complexes. *Trends Cell Biol* 24: 35–43, 2014.

Kofuji T, Fujiwara T, Sanada M, Mishima T, Akagawa K. HPC-1/syntaxin 1A and syntaxin 1B play distinct roles in neuronal survival. *J Neurochem* 130: 514–525, 2014.

Liu Y, Sugiura Y, Lin W. The role of synaptobrevin1/VAMP1 in Ca^{2+}-triggered neurotransmitter release at the mouse neuromuscular junction. *J Physiol* 589: 1603–1618, 2011.

Martin AR. A further study of the statistical composition on the end-plate potential. *J Physiol* 130: 114–122, 1955.

Mishima T, Fujiwara T, Sanada M, Kofuji T, Kanai-Azuma M, Akagawa K. Syntaxin 1B, but not syntaxin 1A, is necessary for the regulation of synaptic vesicle exocytosis and of the readily releasable pool at central synapses. *PLoS One* 9: e90004, 2014.

Mitchell SJ, Ryan TA. Munc18-dependent regulation of synaptic vesicle exocytosis by syntaxin-1A in hippocampal neurons. *Neuropharmacology* 48: 372–380, 2005.

Nichol PF, Botham R, Saijoh Y, Reeder AL, Zaremba KM. A more efficient method to generate null mutants using Hprt-Cre with floxed alleles. *J Ped Surg* 46: 1711–1719, 2011.

Nonet ML, Saifee O, Zhao H, Rand JB, Wei L. Synaptic transmission deficits in *Caenorhabditis elegans* synaptobrevin mutants. *J Neurosci* 18: 70–80, 1998.

Nystuen AM, Schwendinger JK, Sachs AJ, Yang AW, Haider NB. A null mutation in VAMP1/synaptobrevin is associated with neurological defects and prewean mortality in the lethal-wasting mouse mutant. *Neurogenetics* 8: 1–10, 2007.

Peng L, Liu H, Ruan H, Tepp WH, Stoothoff WH, Brown RH, Johnson EA, Yao WD, Zhang SC, Dong M. Cytotoxicity of botulinum neurotoxins reveals a direct role of syntaxin 1 and SNAP-25 in neuron survival. *Nat Commun* 4: 1472, 2013.

Rizo J, Rosenmund C. Synaptic vesicle fusion. *Nat Struct Mol Biol* 15: 665–674, 2008.

Rizo J, Südhof TC. The membrane fusion enigma: SNAREs, Sec1/Munc18 proteins, and their accomplices–guilty as charged? *Annu Rev Cell Dev Biol* 28: 279–308, 2012.

Rosenmund C, Stevens CF. Definition of the readily releasable pool of vesicles at hippocampal synapses. *Neuron* 16: 1197–1207, 1996.

Ruiz R, Casanas JJ, Torres-Benito L, Cano R, Tabares L. Altered intracellular Ca^{2+} homeostasis in nerve terminals of severe spinal muscular atrophy mice. *J Neurosci* 30: 849–857, 2010.

Ruiz-Montasell B, Aguado F, Majó G, Chapman ER, Canals JM, Marsal J, Blasi J. Differential distribution of syntaxin isoforms 1A and 1B in the rat central nervous system. *Eur J Neurosci* 8: 2544–2552, 1996.

Saifee O, Wei L, Nonet ML. The *Caenorhabditis elegans* unc-64 locus encodes a syntaxin that interacts genetically with synaptobrevin. *Mol Biol Cell* 9: 1235–1252, 1998.

Sakaba T, Stein A, Jahn R, Neher E. Distinct kinetic changes in neurotransmitter release after SNARE protein cleavage. *Science* 309: 491–494, 2005.

Schoch S, Deák F, Königstorfer A, Mozhayeva M, Sara Y, Südhof TC, Kavalali ET. SNARE function analyzed in synaptobrevin/VAMP knockout mice. *Science* 294: 1117–1122, 2001.

Schubert J, Siekierska A, Langlois M, May P, Huneau C, Becker F, Muhle H, Suls A, Lemke JR, de Kovel CG, Thiele H, Konrad K, Kawalia A, Toliat MR, Sander T, Rüschendorf F, Caliebe A, Nagel I, Kohl B, Kecskés A, Jacmin M, Hardies K, Weckhuysen S, Riesch E, Dorn T, Brilstra EH, Baulac S, Møller RS, Hjalgrim H, Koeleman BP; EURO-EPINOMICS RES Consortium, Jurkat-Rott K, Lehman-Horn F, Roach JC, Glusman G, Hood L, Galas DJ, Martin B, de Witte PA, Biskup S, De Jonghe P, Helbig I, Balling R, Nürnberg P, Crawford AD, Esguerra CV, Weber YG, Lerche H. Mutations in STX1B, encoding a presynaptic protein, cause fever-associated epilepsy syndromes. *Nat Genet* 46: 1327–1332, 2014.

Schulze KL, Broadie K, Perin MS, Bellen HJ. Genetic and electrophysiological studies of Drosophila syntaxin-1A demonstrate its role in nonneuronal secretion and neurotransmission. *Cell* 80: 311–320, 1995.

Sørensen JB, Nagy G, Varoqueaux F, Nehring RB, Brose N, Wilson MC, Neher E. Differential control of the releasable vesicle pools by SNAP-25 splice variants and SNAP-23. *Cell* 114: 75–86, 2003.

Toonen RF, Wierda K, Sons MS, de Wit H, Cornelisse LN, Brussaard A, Plomp JJ, Verhage M. Munc18-1 expression levels control synapse recovery by regulating readily releasable pool size. *Proc Natl Acad Sci USA* 103: 18332–18337, 2006.

Varoqueaux F, Sons MS, Plomp JJ, Brose N. Aberrant morphology and residual transmitter release at the Munc13-deficient mouse neuromuscular synapse. *Mol Cell Biol* 25: 5973–5984, 2005.

Venken KJ, He Y, Hoskins RA, Bellen HJ. P[acman]: a BAC transgenic platform for targeted insertion of large DNA fragments in *D. melanogaster*. *Science* 314: 1747–1751, 2006.

Vilinsky I, Stewart BA, Drummond J, Robinson I, Deitcher DL. A Drosophila SNAP-25 null mutant reveals context-dependent redundancy with SNAP-24 in neurotransmission. *Genetics* 162: 259–271, 2002.

Washbourne P, Thompson PM, Carta M, Costa ET, Mathews JR, Lopez-Benditó G, Molnár Z, Becher MW, Valenzuela CF, Partridge LD, Wilson MC. Genetic ablation of the t-SNARE SNAP-25 distinguishes mechanisms of neuroexocytosis. *Nat Neurosci* 5: 19–26, 2002.

Zhou P, Pang ZP, Yang X, Zhang Y, Rosenmund C, Bacaj T, Südhof TC. Syntaxin-1 N-peptide and Habc-domain perform distinct essential functions in synaptic vesicle fusion. *EMBO J* 32: 159–171, 2013.